A Case Study on the Attitude Control of the VLS-1 Launcher in the Vibratory Regime*

1st Antonio Silveira
Postgraduate Program in Electrical Engineering
Federal University of Pará
Belém, Brazil
asilveira@ufpa.br

2nd Marco Sagliano
Department of Navigation and Control
German Aerospace Center
Bremen, Germany
marco.sagliano@dlr.de

3rd Rufin Azonsivo
Postgraduate Program in Electrical Engineering
Federal University of Pará
Belém, Brazil
rufin.azonsivo@itec.ufpa.br

4th Matheus Morais da Silva
Postgraduate Program in Electrical Engineering
Federal University of Pará
Belém, Brazil
matheus.morais@itec.ufpa.br

5th Daniel Abreu Macedo da Silva
Postgraduate Program in Electrical Engineering
Federal University of Pará
Belém, Brazil
daniel.abreu@itec.ufpa.br

6th Lucas de Carvalho Sodré
Postgraduate Program in Electrical Engineering
Federal University of Pará
Belém, Brazil
lucas.sodre@itec.ufpa.br

7th Marcos César da Rocha Seruffo
Postgraduate Program in Electrical Engineering
Federal University of Pará
Belém, Brazil
seruffo@ufpa.br

8th David Seelbinder
Department of Navigation and Control
German Aerospace Center
Bremen, Germany
david.seelbinder@dlr.de

9th João Viana da Fonseca Neto
Postgraduate Program in Aerospace Engineering
Federal University of Maranhão
Belém, Brazil
joao.fonseca@ufma.br

10th Stephan Theil
Department of Navigation and Control
German Aerospace Center
Bremen, Germany
stephan.theil@dlr.de

***Abstract*—In this case study, the design and analysis of the attitude control of a rocket based on the Brazilian satellite launch vehicle known as VLS-1 is presented. The simulation model used was of 16th-order, asymmetrical, with coupled dynamics, atmospheric disturbances, actuator saturation, time delay, and bending modes which can be associated with the failure of the VLS-1 that occurred in 1999 when the engine of its second stage exploded after ignition. In this work, we assessed the effects of load disturbances and noises that would strongly interfere with trajectory dispersion, and which might be related to the intense vibratory regime occurring during the maximum dynamic pressure phase of the atmospheric flight of the launcher. The studied control algorithm was a functional digital approximation of the control system reported as the one used in the real VLS-1. The main results were that the control system failed to guarantee stability when simulated in an intense vibratory regime. The theoretical foundation to support the results was that the relative stability margins were smaller than expected in previous designs reported in the literature.**

***Index Terms*—satellite launch system, flight dynamics, attitude control, VLS-1.**

The National Council for Scientific and Technological Development (CNPq) and the Brazilian Federal Agency for Support and Evaluation of Graduate Education (CAPES).

I. Introduction

In this work, the attitude control problem of the Brazilian satellite launch vehicle known as VLS-1 was revisited. This time, studying the controller's relative stability and performance to achieve fast and safe attitude-tracking maneuvers whilst minimizing the intense vibratory regime during the maximum dynamic pressure phase (Max Q) of the atmospheric flight. Based on our simulation results, and supported by theoretical frequency response methods, we demonstrate that the attitude controller of the VLS-1 could have had smaller relative stability margins than expected in previous designs reported in [1], becoming extremely reactive during the intense vibratory regime.

The VLS-1 was the first Brazilian satellite launcher project. Three prototypes were constructed, and a fourth version was initiated but not completed, as the project was canceled in 2016. The third version, VLS-1 V03, marked the downfall of the project in 2003 after a premature ignition of a 1st-stage booster occurred while the vehicle was still inside the assembly building, destroying the facility and killing 21 people, among technicians and engineers, three days prior

to the scheduled launch date. Unfortunately, such a tragic failure eventually obfuscated the advancements achieved by the first two launched prototype versions.

The first version, VLS-1 V01, was launched in 1997, but one of its four boosters of the 1st-stage did not ignite and the vehicle drifted off-course, generating an increased sideslip angle that led the vehicle to an unbearable aerodynamic stress and rupture, 26 seconds after liftoff [2]. The VLS-1 V02 was launched in 1999, and was able to complete the most demanding phases of the atmospheric flight, enduring the transonic and the maximum dynamic pressure regimes, but failed when the 2nd-stage engine was ignited and exploded, around 56 seconds after liftoff [3]. One of the thesis, pointed out in [2], was that the intense vibratory regime may have caused the 2nd-stage explosion. However, he also remarked that there was no conclusive proof of this thesis to date.

In this present case study we investigate this thesis by assessing the attitude control of the VLS-1 in a similar situation as the one faced during the V02 failure, using a detailed simulation model with bending modes, linearized by [4] around the maximum dynamic pressure phase, where the most stressful aerodynamic phenomena occur and the intense vibratory regime could compromise the attitude control stability. For transparency and reproduction, our version of the model can be downloaded from [5]. However, the complete non linear model and its parameters are safeguarded due to confidential matters. How this linearization was performed and what unfavorable consequences could it have when analyzing the failure of the system was not discussed in [4], but the analysis of the unfavorable consequences using this linearized model with simulated sensor noises is one of the contributions of our case study.

The common practice adopted in the real VLS-1 to alleviate the bending modes was to apply notch filters to attenuate the system's gains around the bending mode frequencies. For the VLS-1 at Max Q, two of these modes were identified around 30 and 80 rad/s, both beyond the cutoff frequency of the closed-loop dynamics of the VLS-1 attitude control-loops, so only the first mode was notch-filtered [4].

In [1], published in 2019, the attitude control problem of the VLS-1 was revisited after the cancellation of the project. This work shared important information on the tuning methods and performance's indexes for the controllers. However, in terms of control systems technologies, the procedures were very similar to the ones described in [4] related to the V01 and V02, in which the bending modes alleviation was tackled using notch filters. However, one important fact to remark on is the method the authors selected in [1] to analyze the relative stability. It was based on the frequency response of the open-loop dynamics of an unstable system to assess gain and phase margins, which led them to incorrect robustness indexes expectations, even though the lack of robust performance was apparent, such as negative gain margins, overshoots beyond 20%, too long settling times.

In [6], Yamada, Kienitz, and Ramos revisited in 2024 the VLS-1 attitude control using a technology structured as a Linear Quadratic Gaussian (LQG) with Loop-Transfer-Recovery, demonstrating that the bending modes of the VLS-1 could be alleviated directly by a well-tuned LQG-based attitude controller. Gain and phase margins were also adequately investigated in this work, based on the stable closed-loop system, and robust performance margins were matched to the step response simulations as well, with optimal overshoots and settling times. Differently from the control system design method adopted from the V01 to V03, based on the adaptive control by applying the frozen pole technique as described in [1], just three LQG setups were used during the whole atmospheric flight for the 1st-stage of the VLS-1.

The simulations conducted in [6] utilized a time-varying model, allowing us to observe how the control system behaved during the transonic and max Q phases. By looking at the control signals shown in the paper after the transonic regime and until Max Q [6], it was possible to observe sustained oscillations at the pitch and yaw control signals, possibly with increasing amplitudes and that could give some clues to the thesis raised in [2] for the V02 explosion. We must remark that only load-like wind disturbances were assessed in [6], and our curiosity lies in how noisy wind gusts, generating noisy measurements due to the vibrating structure, along with transport time delay due to the distance between the attitude sensors and the actuators would eventually lead the system to instability.

The main contribution of this work is to revisit the VLS-1 "proportional, integral, *minus* derivative" (PI-D) controller, as described in [1], and study its characteristics in the frequency and time domains during the vibratory regime at Max Q, by using the detailed 16th-order model described in [4], [5].

Beyond this introductory part, this paper is organized as follows: in Sec. II, the VLS-1 model for simulation is presented. In Sec. III, the functional approximation of the VLS-1 PI-D controller and design models are described. The controller design is presented with the tuning based on the linear quadratic method. In Sec. IV, relative stability analysis based on stable closed-loop dynamics is presented. In Sec. V, theoretical results in terms of stability are given and confirmed by simulations. In Sec. VI, the Conclusions are drawn.

II. VLS-1-BASED ATTITUDE MODEL

An image representative of the VLS-1 vehicle is shown in Fig. 1, along with its body system axes, X_b, Y_b, Z_b, and attitude Euler angles, θ, ψ, ϕ. These angles, respective to pitch, yaw, and roll, have positive rotations assuming right-handed rotations with the thumb aligned with the axes arrows.

In order to guide the launcher along its desired trajectory, the Euler angles are controlled using movable nozzles as system actuators. In Fig. 1, visible nozzles are shown at the bottom of the rocket, with the smaller ones respective to the four boosters of the 1st-stage, strapped around the bigger one of the 2nd-stage in the center. The four nozzles of the 1st-stage operate together as described in [2]. Effectively, their movement can be addressed to three virtual nozzle angular deflections, β_θ, β_ψ, β_ϕ, which actuates predominantly on θ, ψ, ϕ, respectively, despite adverse dynamic couplings of this 3-input, 3-output multivariate system.

The VLS-1 models as described in [4] use the mks unit system (meter, kilogram, second), with angles given in

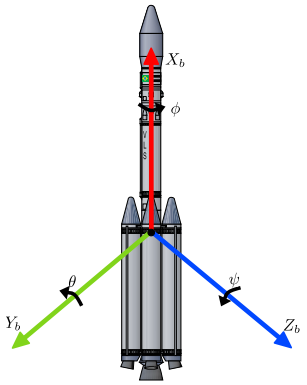

Fig. 1. VLS-1 body system axes, X_b, Y_b, Z_b, and attitude angles, θ (pitch), ψ (yaw), ϕ (roll).

radians (rad). Thus, any results in this work showing angular deflections in degrees, are due to conversion from radians.

To simulate the VLS-1, we considered a slightly modified system (to address sensor noises, delay, and control saturation) based on the model in [4], given by:

$$\dot{\mathbf{x}}(t) = \mathbf{A_c}\mathbf{x}(t) + \mathbf{B_c}\mathbf{sat}[\mathbf{u}(t - t_d)] + \mathbf{G_c}\mathbf{w}(t), \quad (1)$$

$$\mathbf{y}(t) = \mathbf{C}x(t) + \mathbf{v}(t), \quad (2)$$

$$\mathbf{sat}\left[\mathbf{u}(t)\right] = \begin{cases} \mathbf{u}_{\max} & \text{if } \mathbf{u}(t) \geqslant \mathbf{u}_{\max}, \\ \mathbf{u}(t) & \text{if } \mathbf{u}_{\min} < \mathbf{u}(t) < \mathbf{u}_{\max}, \\ \mathbf{u}_{\min} & \text{if } \mathbf{u}(t) \leqslant \mathbf{u}_{\min}. \end{cases} \quad (3)$$

The state vector $\mathbf{x}(t) \in \mathbb{R}^{16}$ is comprised of the following state variables (with $\mathbf{x^T}(t)$ as the transpose of $\mathbf{x}(t)$):

$$\mathbf{x^T}(t) = \left[\begin{array}{cccccccc} w & q & \theta & \theta_{b_{11}} & \theta_{b_{12}} & \theta_{b_{21}} & \theta_{b_{22}} & v \\ r & \psi & \psi_{b_{11}} & \psi_{b_{12}} & \psi_{b_{21}} & \psi_{b_{22}} & p & \phi \end{array} \right]. \quad (4)$$

v, and w, are the linear velocity components relative to Y_b and Z_b; p, q, and r, the angular velocities relative to rotations about X_b, Y_b, and Z_b; $\theta_{b_{11}}$, and $\theta_{b_{21}}$, the 1st and 2nd bending modes of $\theta(t)$; $\theta_{b_{12}}$, and $\theta_{b_{22}}$, the time-derivative of the 1st and 2nd bending modes of $\theta(t)$; $\psi_{b_{11}}$, and $\psi_{b_{21}}$, the 1st and 2nd bending modes of $\psi(t)$; $\psi_{b_{12}}$, and $\psi_{b_{22}}$, the time-derivative of the 1st and 2nd bending modes of $\psi(t)$.

The input vector is $\mathbf{u^T}(t) = \left[\begin{array}{ccc} \beta_\theta & \beta_\psi & \beta_\phi \end{array} \right]$ and is related to the nozzle angular deflections in radians. Positive nozzle deflections on β_θ and β_ϕ generate positive rotations on θ (pitch) and ϕ (roll), while β_ψ operates inversely on ψ (yaw). A detailed explanation of how such a coordinate system is defined is shown in [2], [4].

The disturbance vector $\mathbf{w^T}(t) = \left[\begin{array}{cc} w_\theta & w_\psi \end{array} \right]$ is an input vector, related to wind disturbances given in meters per second, affecting predominantly the pitch and yaw. The sensor-measured output vector is $\mathbf{y^T}(t) = \left[\begin{array}{ccc} \theta & \psi & \phi \end{array} \right]$, given in radians, and the sensor noise vector is $\mathbf{v^T}(t) = \left[\begin{array}{ccc} v_\theta & v_\psi & v_\phi \end{array} \right]$, simulated as Gaussian noises.

The system model is assumed to be non-linear with control saturation of $\pm 4°$ on the nozzle deflection [1], represented by $\mathbf{u}_{\min}$ and $\mathbf{u}_{\max}$. The system also incorporates the simulation of an input delay $t_d = 5$ milliseconds to simulate non-collocated sensor-actuator dynamics [7], due to their distance from top to bottom, and due to digital processing and communication delays.

The system matrices, $\mathbf{A_c}$, $\mathbf{B_c}$, $\mathbf{G_c}$, $\mathbf{C}$, along with a long list of 36 parameters, were omitted in this work, but these can be obtained from the Appendix A in [4]. However, in [4] the bending modes were not enabled and the $\mathbf{A_c}$ matrix was modified in the following elements $a_{i,j}$ (i-row, j-column): $a_{3,4}, a_{3,6}, a_{10,11}, a_{10,13}$, changing their values from 0 to 1.

To assess the digital controllers considered in this case study, the simulation model was converted to the discrete-time domain k using the zero-order-hold method, being rewritten as follows:

$$\begin{aligned} \mathbf{x}(k) &= \mathbf{A}\mathbf{x}(k-1) + \mathbf{B}\mathbf{sat}\left[\mathbf{u}(k-d)\right] + \mathbf{G}\mathbf{w}(k-1), \\ \mathbf{y}(k) &= \mathbf{C}\mathbf{x}(k) + \mathbf{v}(k). \end{aligned} \quad (5)$$

$d = 1 + \lceil t_d/T_s \rceil$, with the ceiling operator $\lceil . \rceil$, is the positive integer discrete time delay based on the continuous-time delay t_d and the sampling time T_s.

The selection of the sampling frequency for control system design purposes accounted for the two resonant peaks of the bending modes, to allow the controller to be able to tackle them. The fastest poles in the VLS-1 model are related to the 2nd bending mode at 80.4 rad/s. Using the rule of thumb for selecting the sampling frequency ω_s (or in Hertz, $f_s = \frac{\omega_s}{2\pi}$) to be at least 10 times faster than the frequency of interest [8], has led to the sampling time $T_s \leq 0.0078$ seconds.

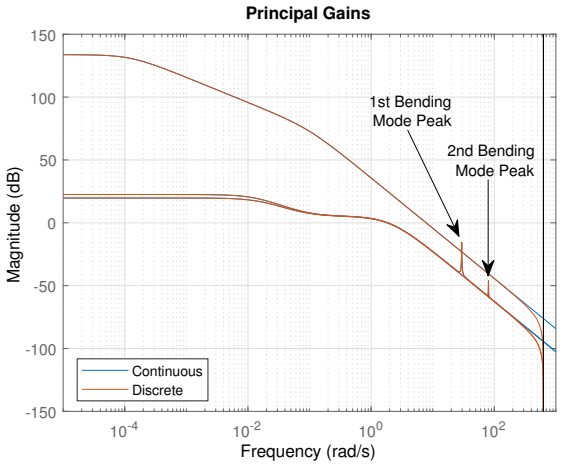

Fig. 2. Principal gains of the continuous and discrete models of the VLS-1. The bending modes resonant peaks occur at 29.5 and 80.4 rad/s, which are well represented by the discrete case using $T_s = 5$ milliseconds.

In Fig. 2, the magnitude plots of the principal gains (or singular values) of the VLS-1 model in the continuous case and the discrete case with $T_s = 5$ milliseconds are shown. The two resonant peaks of the bending modes are well represented by the discrete model, as can be seen from the superimposed magnitude plots.

III. VLS-1 PI-D CONTROLLER AND DESIGN MODELS

The attitude controllers for the VLS-1 V01 and V02 prototypes were of the PI-D type, as reported in [4] and [1]. Such a control structure is ideal to avoid the *derivative kick* (i.e., an impulsive control action) when a sudden step-like attitude reference change occurs. In its control law, the reference signal is not derived, even though the regulatory

properties to tackle output disturbances are the same as in a common PID, as follows:

$$U(s) = \left(k_p + k_i\frac{1}{s}\right)R(s) - \left(k_p + k_i\frac{1}{s} + k_d s\right)Y(s), \tag{6}$$

with k_p, k_i, k_d, the proportional, integral, and derivative gains, and $U(s)$, $R(s)$, $Y(s)$, the control, the reference, and the controlled output signals, respectively.

The VLS-1 PI-D tuning and performance were based on the Linear Quadratic Regulator (LQR) method and simplified 2nd-order models from the Appendix A in [4]:

$$\frac{\theta(s)}{\beta_\theta(s)} = \frac{7.3734}{s^2 - 4.077}, \tag{7}$$

$$\frac{\psi(s)}{\beta_\psi(s)} = \frac{-7.5648}{s^2 - 4.0726}, \tag{8}$$

$$\frac{\phi(s)}{\beta_\phi(s)} = \frac{61.0492}{s^2 + 0.098859s}. \tag{9}$$

A generalization of these 2nd-order models is given by:

$$\frac{Y(s)}{U(s)} = \frac{k_s\omega_n^2}{s^2 + 2\zeta\omega_n s + \omega_n^2}, \tag{10}$$

in which k_s, ω_n, ζ, are the static gain, the natural frequency, and the damping factor. Converting this system to the state-space form using the state vector $\left[\begin{array}{cc} y(t) & \dot{y}(t) \end{array}\right]^{\mathbf{T}}$, leads to

$$\left[\begin{array}{c} \dot{y}(t) \\ \ddot{y}(t) \end{array}\right] = \left[\begin{array}{cc} 0 & 1 \\ -\omega_n^2 & -2\zeta\omega_n \end{array}\right]\left[\begin{array}{c} y(t) \\ \dot{y}(t) \end{array}\right] + \left[\begin{array}{c} 0 \\ k_s\omega_n^2 \end{array}\right]u(t). \tag{11}$$

Now, converting the PI-D, in (6), to the time-domain,

$$u(t) = k_p\left[r(t) - y(t)\right] + k_i\int\left[r(t) - y(t)\right]dt - k_d\dot{y}(t), \tag{12}$$

it is possible to correlate its control law and the state vector, and also the controller's integral term,

$$e_i(t) = \int\left[r(t) - y(t)\right]dt, \tag{13}$$

as a new state variable, augmenting the system state space realization to the following form:

$$\left[\begin{array}{c} \dot{y}(t) \\ \ddot{y}(t) \\ \dot{e}_i(t) \end{array}\right] = \left[\begin{array}{ccc} 0 & 1 & 0 \\ -\omega_n^2 & -2\zeta\omega_n & 0 \\ -1 & 0 & 0 \end{array}\right]\left[\begin{array}{c} y(t) \\ \dot{y}(t) \\ e_i(t) \end{array}\right] + \left[\begin{array}{c} 0 \\ k_s\omega_n^2 \\ 0 \end{array}\right]u(t) + \left[\begin{array}{c} 0 \\ 0 \\ 1 \end{array}\right]r(t). \tag{14}$$

Assuming the LQR control law when $r(t) = 0$ to be

$$u(t) = -\mathbf{K}\left[\begin{array}{ccc} y(t) & \dot{y}(t) & e_i(t) \end{array}\right]^{\mathbf{T}}, \tag{15}$$

the LQR gain has the optimal PI-D gains as follows:

$$\mathbf{K} = \left[\begin{array}{ccc} k_p & k_d & -k_i \end{array}\right]. \tag{16}$$

The LQR state and control optimization weighting matrices were set as specified in [1]: $\mathbf{Q} = diag\left(\begin{array}{ccc} 0.1 & 1 & 0.2 \end{array}\right)$ and $\mathbf{R} = 0.4$. Then, assuming the LQR gain solution as a standardized method available in several control systems toolboxes as a function of the form $\mathbf{K} = lqr\left(\mathbf{A_c}, \mathbf{B_c}, \mathbf{Q}, \mathbf{R}\right)$, the obtained gains for the pitch, yaw, roll, were:

$$\begin{aligned} \mathbf{K}_\theta &= \left[\begin{array}{ccc} 2.3009 & 1.7675 & -0.7071 \end{array}\right], \\ \mathbf{K}_\psi &= \left[\begin{array}{ccc} -2.2793 & -1.7614 & 0.7071 \end{array}\right], \\ \mathbf{K}_\phi &= \left[\begin{array}{ccc} 1.5840 & 1.5958 & -0.7071 \end{array}\right]. \end{aligned} \tag{17}$$

To simplify the analysis, these PI-D systems were rewritten in a generalized reference-signal-tracking (RST) form [8]:

$$u(k) = \frac{E(z)r(k) - F(z)y(k)}{\Delta(z)}, \tag{18}$$

where the discrete-time approximation for the PI-D systems was obtained using the backward difference method, leading to the following set of polynomials, based on k_p, k_i, k_d, T_s, defined in the discrete-time shift operator domain, z:

$$\Delta(z) = 1 - z^{-1}, \tag{19}$$

$$E(z) = \left(k_p + k_i T_s\right) + \left(-k_p\right)z^{-1}, \tag{20}$$

$$F(z) = \left(k_p + k_i T_s + \frac{k_d}{T_s}\right) + \left(-k_p - 2\frac{k_d}{T_s}\right)z^{-1} + \left(\frac{k_d}{T_s}\right)z^{-2}. \tag{21}$$

IV. Relative stability analysis

Let us assume a generalized zero-order-hold equivalent system for the design models in (7) to (9), with an output disturbance $v(k)$, as being:

$$y(k) = \frac{B(z)}{A(z)}z^{-1}u(k) + v(k). \tag{22}$$

By substituting the control law in (18) into (22), the closed-loop system is given by:

$$y(k) = \frac{\left[B(z)E(z)z^{-1}\right]r(k) + \left[\Delta(z)A(z)\right]v(k)}{\Delta(z)A(z) + B(z)F(z)z^{-1}}. \tag{23}$$

By considering null initial conditions, these transfer function models in the discrete-time domain can also be analyzed in the discrete frequency domain, $z = e^{j\omega T_s}$, $\omega \in \mathbb{R}^+$.

The relative stability analysis can be assessed by frequency response methods, so to evaluate how the designed control system, from the reference $r(k)$ to the output $y(k)$, attenuates the effects from the disturbance $v(k)$ to $y(k)$. In this sense, we define the closed-loop sensitivity as $S(z)$ and the complementary sensitivity as $T(z)$, so that

$$Y(z) = T(z)R(z) + S(z)V(z). \tag{24}$$

If (and only if) (24) is stable, then the magnitude plots of the sensitivity and co-sensitivity, $|S(e^{j\omega T_s})|$ and $|T(e^{j\omega T_s})|$, can be analyzed as in the example shown in Fig. 3. In this figure, a disturbance sensitivity peak around 2 dB is strongly attenuated by a co-sensitivity of -10 dB.

Compared to Bode-based open-loop relative stability analysis, this closed-loop method is of paramount importance for case studies such as the VLS-1, due to its unstable characteristic and the fact that its PI-D controller is a 2-degrees-of-freedom controller, i.e. the reference filter differs from the feedback filter as shown in (6) and (18). Thus, the closed-loop analysis is indispensable, while the open-loop analysis is incorrect since an open-loop unstable system does not respond sinusoidally to sinusoidal inputs.

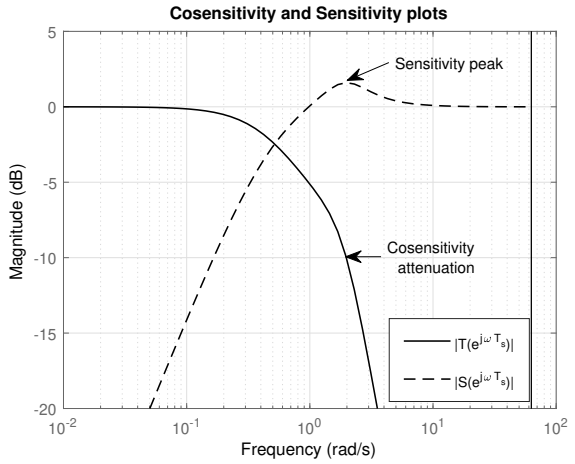

Fig. 3. Example of magnitude attenuation of the frequencies where the disturbance sensitivity is high.

Beyond the graphical interpretation of relative stability and robustness based on the magnitude plots, it is also possible to quantify these results based on gain margin and phase margin, as follows [9]:

$$G_{M_{dB}} \geqslant \min\left[20\log_{10}\left(\frac{m_s}{m_s-1}\right), 20\log_{10}\left(1+\frac{1}{m_t}\right)\right], \tag{25}$$

$$P_{M_{\deg}} \geqslant \left(\frac{180^\circ}{\pi}\right)\min\left\{\left[2\sin^{-1}\left(\frac{1}{2m_s}\right)\right], \left[2\sin^{-1}\left(\frac{1}{2m_t}\right)\right]\right\}, \tag{26}$$

$$m_t = \max_{\omega}\left|T(e^{j\omega T_s})\right|, \tag{27}$$

$$m_s = \max_{\omega}\left|S(e^{j\omega T_s})\right|, \tag{28}$$

with m_s and m_t being the linear amplitude peaks of these sensitivity functions.

A rule of thumb for selecting relative stability margins lies in the trade-off between safety and performance: the robust performance. These margin requirements may differ between fields of application, but in general, these are similar to the range presented in the aerospace field [10]: 6 to 15 dB, and 30° to 60°. However, smaller margins addressed as robust performance margins can also be found, as in [9]: 4.6 to 12 dB, and 30° to 45°.

V. Results

In this section, we begin by evaluating the relative stability based on the 2nd-order design models, analyzing the sensitivity functions and the robustness by gain and phase margins. Then, we continue to the simulation part with the 16th-order model, presenting the system's closed-loop step response without any wind disturbances or measurement noises. This is followed by a 50 seconds simulation with load-like wind disturbances while applying pitch-over and roll program maneuvers based on the guidance data presented in [6]. Then, these same simulations are repeated with attitude noises, causing the vehicle to lose stability.

A. Relative stability and robustness results

Using the relative stability analysis shown in the previous section, the sensitivity functions for all three PI-D controllers are shown in Fig. 4. The pitch and yaw cases were practically equivalent due to their symmetry with regards to the design models in (7) and (8), and the same LQR optimization performance. Their sensitivity to disturbances was considerably high near 1 rad/s, and the co-sensitivity was still above 0 dB. At the frequencies of the bending modes resonant peaks, previously shown in Fig. 2, near 30 and 80 rad/s, the average attenuation was of 34 and 51 dB, respectively. The roll case has exhibited a better set of sensitivity functions. The controllers' bandwidth, quantified as the frequencies of -3 dB co-sensitivity attenuation, were 1.93, 1.92, and 1.41 rad/s, for pitch, yaw, and roll, respectively.

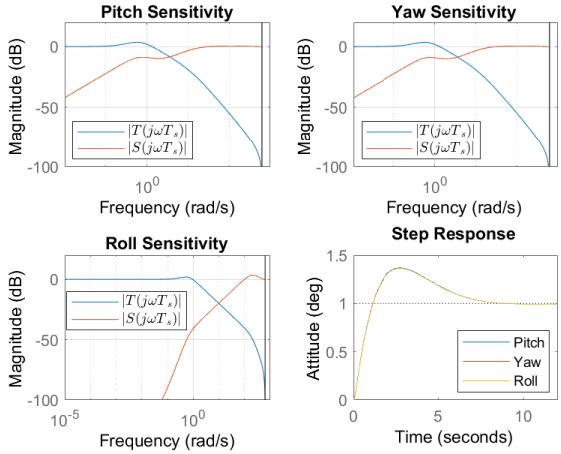

Fig. 4. Sensitivity functions and unit step response for the pitch, yaw, roll, based on their respective 2nd-order design models. The controllers' bandwidth, quantified as the frequencies of -3 dB co-sensitivity attenuation, were 1.93, 1.92, and 1.41 rad/s, for pitch, yaw, and roll.

TABLE I
Gain Margins, Phase Margins and Sensitivity Peaks

Margins	*Pitch*	*Yaw*	*Roll*
$G_{M_{dB}} \geqslant$	4.3988 dB	4.4123 dB	5.1055 dB
$P_{M_{\deg}} \geqslant$	38.4989°	38.6550°	39.0306°
m_t	1.5166	1.5107	1.2500
m_s	1.0599	1.0612	1.4967

The gain margins and phase margins for the three control loops are shown in Table I. The obtained minimal margins were too small and out of the robust performance range, but they match with the sensitivity plots in Fig. 4 and with the unit step response shown in the fourth subplot in the same figure. This unit step response can be said to be identical to the one presented in [1] (they differ slightly due to the use of the transonic model, while we are using the model at max Q). This confirms that the designed controllers are functional approximations of the PI-D of the VLS-1. It is important to add that in [1], gain and phase margins were obtained by Bode-based analysis in open-loop, probably leading to incorrect gain and phase margins obtained by means of an algorithmic tool without the appropriate critic correlation between robust margins and robust step response, neglecting

negative gain margins and overshoots beyond 20% as a warning sign that something was probably wrong.

For the purpose of comparison, we have reproduced the open-loop Bode plot from [1], as shown in Fig. 5, where the authors used the unstable transfer function:

$$G_{ol}(s) = \left(\frac{k_p s + k_i}{s}\right)\left[\frac{\theta(s)}{\beta_\theta(s)}\right](k_d s + 1)\,. \qquad (29)$$

It must be remarked that the term $(k_d s + 1)$ comes form the feedback part of the PI-D control-loop, thus it was also improper to use it for the open-loop analysis.

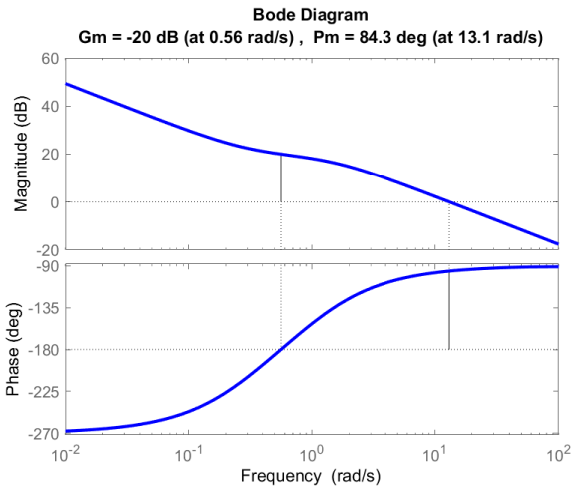

Fig. 5. Incorrect gain and phase margins based on the Bode plot of an unstable direct loop. Reproduction based on the controller and plant parameters in [1].

The gain margin in [1] was in fact negative, as is clearly visible in Fig. 5.

From the results obtained in our work, we can conclude that these attitude controllers did not have the robustness margins that were previously considered in [1]. Based on the more demanding robust performance margins from the aerospace field [10], or on less demanding ones from the process control field [9], these PI-D attitude controllers exhibited poor relative stability margins (cf. Tab. I).

B. Simulation results with the 16th-order model

We assessed the 16th-order simulation model using simultaneous unit-step reference changes. During this test, it was not used load-like wind disturbances or noise-like gust winds. These results are exhibited in figures 6 and 7.

In figures 6 and 7, the controlled outputs and control signals are shown for the simultaneous reference change. The expected overshoots beyond 20% were also observed. The amplitude of the control signals was within the limits of $\pm 4°$, however, it is clearly visible the sustained oscillations being passed on to the actuators, and this was similar to the observed oscillations in the control signals exhibited in [6], even though such oscillations were barely visible in the pitch and yaw step responses output measurements.

Figure 8 is based on the guidance data presented in [6], showing a roll program maneuver followed by the pitch-over maneuver, a few seconds after liftoff. The control signals that generated these results are shown in Fig. 9. In this simulation, load-like wind disturbances were applied with the

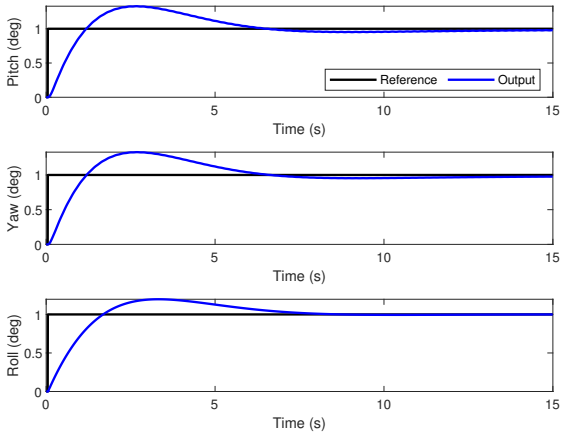

Fig. 6. Closed-loop unit step response using the 16th-order non-linear model with bending modes. Case with simultaneous reference changes.

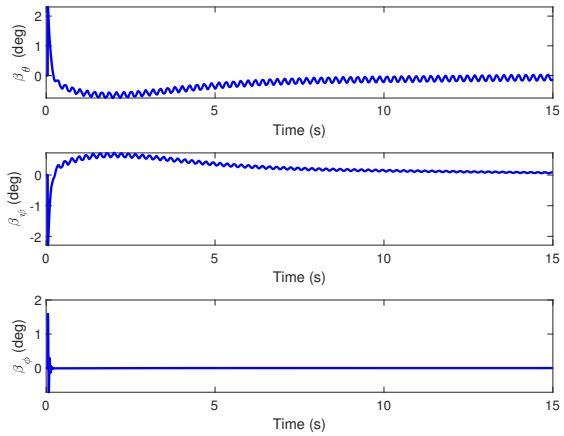

Fig. 7. Control signals of the closed-loop unit step response simulation using the 16th-order non-linear model with bending modes. Case with simultaneous reference changes. Pitch and yaw control signals with apparent sustained oscillations.

same magnitudes and at the same instants as shown in [6]. A step of 6 m/s was simultaneously applied at liftoff to both pitch and yaw and then a 20 m/s step was also simultaneously applied at the instant 10 s. It is possible to observe in detail the effects of these disturbances, especially by looking at the yaw angle. The angular dispersion is acceptable according to the error limit of $\pm 0.5°$ when not executing the roll maneuver [6]. Even though, the high overshoot and long settling times have increased the time to recover after the second wind disturbances have hit the vehicle.

Despite the time to recover from the disturbances being considerably long, all control signals were within the saturation limits of $\pm 4°$ as discussed in [1].

The wind disturbances test with PI-D shown in figures 8 and 9 presented inferior results if compared to the LQG in [6], but still, the vehicle has maintained stability under low-frequency disturbances. The new test proposed in this work, however, is to include zero mean Gaussian noises, assessing the case of normal distribution disturbances or equal power disturbances affecting the whole sampled spectrum, thus assuming an intense vibratory regime with both structural

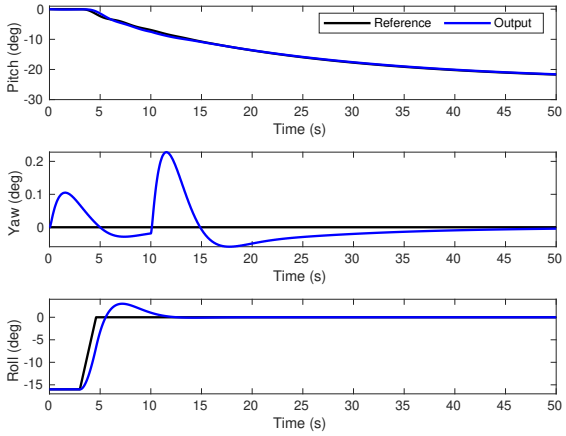

Fig. 8. Roll program and pitch-over maneuvers based on the guidance data shown in [6]. 6 m/s winds at liftoff and 20 m/s at 10 seconds were applied to pitch and yaw.

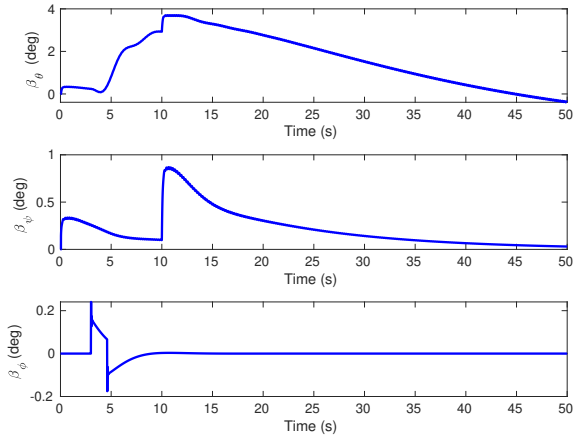

Fig. 9. Control signals used to execute the roll program and pitch-over maneuvers based on the guidance data shown in [6]. In this case, the vehicle is under the influence of 6 m/s winds at liftoff and 20 m/s winds at 10 seconds after liftoff. The oscillations in the control signals are barely visible but are still present.

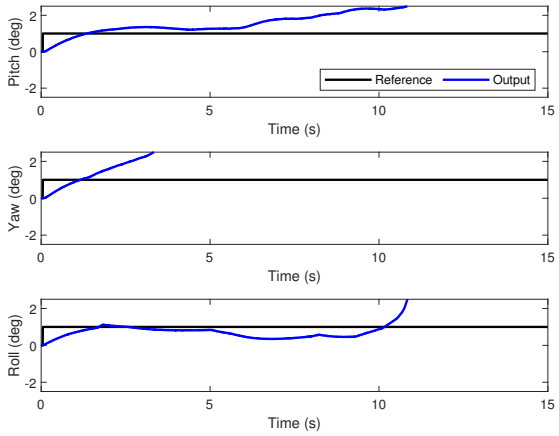

Fig. 10. Closed-loop unit step response using the 16th-order non-linear model with bending modes. Case with simultaneous reference changes and measurement noises with a linear power of $\sigma^2_{\mathbf{v}} = 2.5 \times 10^{-9}$. The vehicle became unstable.

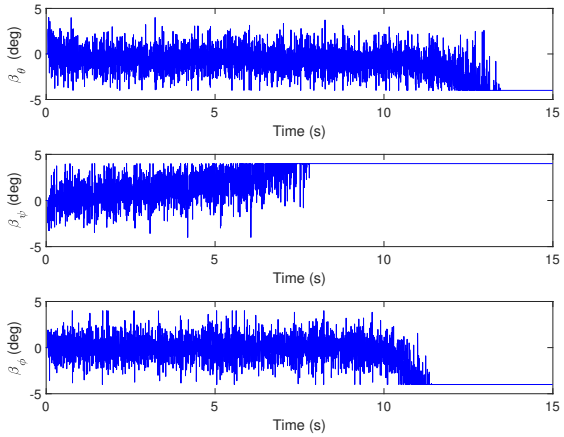

Fig. 11. Control signals of the closed-loop unit step response simulation using the 16th-order non-linear model with bending modes. Control signals with saturation and strong chattering due to the intense vibratory simulation. The vehicle became unstable.

oscillations and sensor noise.

The results for the tests simulating the intense vibratory regime are shown in figures 10 and 11 for the unit-step response case without load-like disturbances, and in figures 12 and 13 for the case with roll program, pitch-over maneuver, and wind disturbances. In both cases, we have lost stability. The zero mean Gaussian noises used in these simulations were generated with a linear power of $\sigma^2_{\mathbf{v}} = 2.5 \times 10^{-9}$ $(rad/h)^2$ and $\sigma^2_{\mathbf{v}} = 10^{-10}$ $(rad/h)^2$, for the unit step response without loads and for the roll program and pitch-over with winds, respectively.

In Fig. 14, it is shown the noises applied to the roll program and pitch-over simulation. Their variances were selected by trial and error increments to find out the values which would generate instability. However, these values were found to be way bellow the noise power of real angular sensors technologies. For example, in a 2022 study on Interferometric Fiber Optic Gyroscope (IFOG) applied to the Brazilian Microsatellite Launch Vehicle, VLM-1, the standard deviation $\sigma_{\mathbf{v}}$ in degrees per hour, calculated based on the angular random walk, $\mathbf{v}_{\text{ARW}} = 5.4 \times 10^{-4}\ ^\circ/\sqrt{h}$, in the frequency bandwidth $f_{BW} = 5$ Hz, was given by [11]:

$$\sigma_{\mathbf{v}} = \mathbf{v}_{\text{ARW}} \left(60\sqrt{f_{\text{BW}}}\right). \tag{30}$$

Assuming IFOG gyroscopes, the theoretical Gaussian noise power would be of $\sigma^2_{\mathbf{v}} = 5.2 \times 10^{-3}\ (^\circ/h)^2$ or $\sigma^2_{\mathbf{v}} \approx 10^{-5}$ $(rad/h)^2$, thus higher than the noises shown in Fig. 14.

It is important to observe that the noises used in our simulations were of extremely low power, barely visible in the attitude angles, thus reinforcing possible problems such as the lack of relative stability margins in the linear quadratic tuning of the PI-D presented in this study and in [1].

VI. Conclusions

In this work, the VLS-1 attitude control problem was revisited, assessing the thesis pointed out in [2] that the VLS-1 V02 failure in 1999 could have been related to the intense vibratory regime during the maximum dynamic pressure

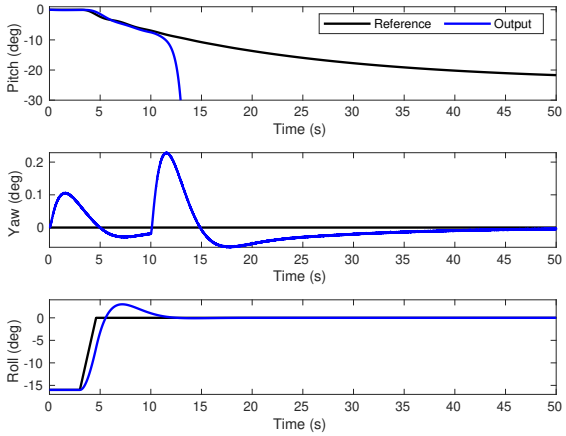

Fig. 12. Roll program and pitch-over maneuvers based on the guidance data shown in [6]. 6 m/s winds at liftoff and 20 m/s at 10 seconds were applied to pitch and yaw, during the intense vibratory regime simulated by Gaussian noises using a linear power of $\sigma^2_{\mathbf{v}} = 1 \times 10^{-10}$. The vehicle became unstable.

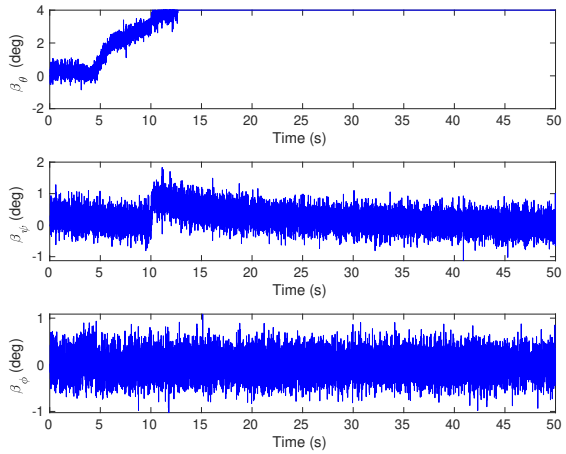

Fig. 13. Control signals used to execute the roll program and pitch-over maneuvers. In this case, the vehicle is under the influence of 6 m/s winds at liftoff and 20 m/s winds at 10 seconds after liftoff. The intense vibratory regime generated intense control signal chattering and saturation. The vehicle became unstable.

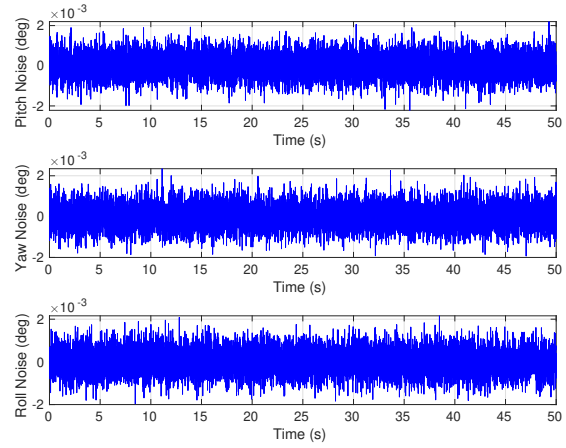

Fig. 14. Zero mean Gaussian noises applied to the roll program and pitch-over maneuvers simulation. With peaks of $\pm 0.002°$, these noises eventually led the vehicle to lose stability.

phase. In our study, we considered the PI-D control technology as described in [4] and [1], using the linear quadratic tuning described in these previous works. We observed that the robustness margins in [1] were in fact smaller than what was expected, and out of the robust performance range. When the designed controllers were put to test with the 16th-order non-linear model simulating the scenario of a vibratory regime, the VLS-1 model exhibited strong control signal chattering, leading to an equivalent nozzle intense vibratory regime, control saturation, and finally, instability.

This is an ongoing study on guidance and control of satellite launch vehicles, still focusing on previous works related to the Brazilian space program, and looking forward to proposing follow-up works dealing with parametric time-varying simulations, the assessment of different proportional-integral-derivative control topologies and tunings, the LQG and model predictive control, in order to avoid the unstable outcome observed in this work.

ACKNOWLEDGMENT

The authors from the Federal University of Pará thank the National Council for Scientific and Technological Development (CNPq), and the Brazilian Federal Agency for Support and Evaluation of Graduate Education (CAPES), for the financial support.

REFERENCES

[1] F. O. Silva, W. d. C. Leite Filho, A. G. Brito, and A. G. d. Silva, "Tuning techniques evaluation for satellite launch vehicle attitude controllers," *Journal of Aerospace Technology and Management*, vol. 11, p. e2419, 2019. [Online]. Available: https://doi.org/10.5028/jatm.v11.1004

[2] A. F. Palmerio, *Introdução à Tecnologia de Foguetes*, 2nd ed. SindCT, São José dos Campos - SP, 2017. [Online]. Available: https://sindct.org.br/sindct/comunicacao/livros-e-cartilhas/introducao-a-tecnologia-de-foguetes/

[3] Retro-Space-HD, "VLS-1 V2 launch failure - solid fuel Brazilian rocket, 1999, Alcantara Space Center," May 2022. [Online]. Available: https://www.youtube.com/watch?v=6kx7EHqtG6Q

[4] F. de Oliveira Ramos, "Automation of H_∞ controller design and its observer-based realization," Ph.D. dissertation, Instituto Nacional de Pesquisas Espaciais (INPE), Institut Supérieur de l'Aéronautique et de l'Espace (ISAE), São José dos Campos (Brasil), Toulouse (França), 2011.

[5] A. Silveira, M. Sagliano, R. Azonsivo, M. Seruffo, J. Fonseca-Neto, D. Seelbinder, and S. Theil, "Matlab codes for the attitude control and vls-1 rocket public benchmark model. Published by MATLAB Central File Exchange," www.mathworks.com/matlabcentral/fileexchange/176313-attitude-control-and-vls-1-rocket-public-benchmark-model, 2025, [Online; accessed 11-Feb-2025].

[6] A. F. C. de S. Yamada, K. H. Kienitz, and F. de O. Ramos, "Robust attitude control of a flexible launch vehicle subjected to wind disturbances," in *XXV Brazilian Congress of Automatics (CBA), Rio de Janeiro, RJ, Brazil*, 2024.

[7] B. Wie, W. Du, and M. Whorton, *Analysis and Design of Launch Vehicle Flight Control Systems*. AIAA, 2012. [Online]. Available: https://arc.aiaa.org/doi/abs/10.2514/6.2008-6291

[8] K. J. Astrom and B. Wittenmark, *Computer-controlled systems: theory and design*, 3rd ed. Mineola, NY, USA: Dover Publications, 2011.

[9] D. E. Seborg, T. F. Edgar, and D. A. Mellichamp, *Process Dynamics and Control*, 2nd ed. Hoboken, NJ, USA: John Wiley & Sons, Inc., 2003.

[10] B. L. Stevens, F. L. Lewis, and E. N. Johnson, *Aircraft Control and Simulation: dynamics, controls design, and autonomous systems*, 3rd ed. Hoboken, NJ, USA: John Wiley & Sons, Inc., 2016.

[11] G. Nunes, A. Carvalho, A. T. Júnior, L. Vito, J. ao Sakamoto, and N. Oliveira, "Simulation of an interferometric fiber optic gyroscope applied to a rocket model," in *Simpósio de Aplicações Operacionais em Áreas de Defesa (SIGE)*, 2022.